

NANO EXPRESS

Open Access

Enhanced resistive switching memory characteristics and mechanism using a Ti nanolayer at the W/TaO_x interface

Amit Prakash¹, Siddheswar Maikap^{1*}, Hsien-Chin Chiu¹, Ta-Chang Tien² and Chao-Sung Lai¹

Abstract

Enhanced resistive memory characteristics with 10,000 consecutive direct current switching cycles, long read pulse endurance of $>10^5$ cycles, and good data retention of $>10^4$ s with a good resistance ratio of $>10^2$ at 85°C are obtained using a Ti nanolayer to form a W/TiO_x/TaO_x/W structure under a low current operation of 80 μA, while few switching cycles are observed for W/TaO_x/W structure under a higher current compliance >300 μA. The low resistance state decreases with increasing current compliances from 10 to 100 μA, and the device could be operated at a low RESET current of 23 μA. A small device size of 150×150 nm² is observed by transmission electron microscopy. The presence of oxygen-deficient TaO_x nanofilament in a W/TiO_x/TaO_x/W structure after switching is investigated by Auger electron spectroscopy. Oxygen ion (negative charge) migration is found to lead to filament formation/rupture rather than oxygen vacancy (hole) migration, and it is controlled by Ti nanolayer at the W/TaO_x interface. Conducting nanofilament diameter is estimated to be 3 nm by a new method, indicating a high memory density of ≈ 100 Tbit/in².

Keywords: Resistive switching; W/TaO_x; Ti nanolayer; Oxygen ion migration; Nanofilament

Background

Resistive switching random access memories (RRAM) with simple metal-insulator-metal stacks are under intensive investigation owing to their great promise for use in next-generation memory applications [1-5]. However, their nonuniformity in switching, low yield, and unclear switching mechanism hinder their practical realization. RRAM devices with simple composition, easy fabrication process, and good 3D integration compatibility will be needed in the future. Methods such as doping, formation polarity control, bottom electrode modification, nanocrystal insertion, and interfacial engineering have recently been investigated to improve the characteristics of resistive switching memory [6-10]. Among other important switching materials such as TiO_x [11,12], NiO_x [13], HfO_x [10,13-15], ZrO_x [16-22], Na_{0.5}Bi_{0.5}TiO₃ [23], SrTiO₃ [24], ZnO [25,26], GeO_x [27], and SiO_x [28], tantalum oxide (TaO_x) is one of the most promising choices for

future RRAM applications. However, TaO_x-based RRAM devices are infrequently reported [5,29-34]. Terai et al. [32] used a TiO₂ layer in a Ru/Ta₂O₅/TiO₂/Ru stack with good thermal stability. Ninomiya et al. [33] reported an Ir/Ta₂O_{5-δ}/TaO_x/TaN structure, and Lee et al. [5] reported a Pt/Ta₂O_{5-x}/TaO_{2-x}/Pt crossbar structure with two layers of TaO_x and at least one of the inert electrodes such as Ru, Ir, and Pt. Generally, many researchers use one inert electrode to improve the performance of resistive switching memory [5,34]; however, tungsten (W) as both bottom and top electrodes in a W/TiO_x/TaO_x/W structure has not yet been reported. In this work, a resistive switching memory device using a Ti nanolayer at the W/TaO_x interface and enhanced memory characteristics such as excellent 10,000 consecutive stable dc switching cycles, long read pulse endurance of $>10^5$ cycles, and good data retention of 10^4 s at 85°C with a large resistance ratio of $>10^2$ under a low compliance current (CC) of 80 μA are reported. Furthermore, the device can be operated with a small 'RESET' current of 23 μA. For comparison, the W/TaO_x/W memory device is also fabricated. The device size of 150×150 nm² is observed using a high-resolution transmission

* Correspondence: sidhu@mail.cgu.edu.tw

¹Department of Electronic Engineering, Chang Gung University, Tao-Yuan 333, Taiwan

Full list of author information is available at the end of the article

electron microscope (HRTEM). The thicknesses of TiO_x and TaO_x nanolayers are 3 and 7 nm, respectively. The presence of oxygen-deficient TaO_x conducting filaments is investigated by Auger electron spectroscopy (AES) before and after switching of the memory devices. The switching mechanism of the oxygen ion migration rather than the vacancy migration due to a lower barrier height of electrons is investigated, and a filament diameter of ≈ 3 nm is calculated using a new method also reported in this work. Considering a small filament diameter, a high memory density of ≈ 100 Tbit/in.² could be designed in future.

Methods

W/Ti/TaO_x/W-structured (device S1) and W/TaO_x/W-structured (device S2) resistive switching memory stacks were fabricated. A small via size of 150×150 nm² was

etched into the SiO₂ on the W bottom electrode (BE), which was about 100 nm in thickness. A high- κ Ta₂O₅ film with a thickness ($t_{\text{Ta}_2\text{O}_5}$) of ≈ 7 nm was then deposited by an e-beam evaporator, followed by the sequential deposition of a thin (≈ 3 nm) interfacial layer of titanium (Ti) and ≈ 200 -nm-thick W layer as a top electrode (TE) by rf sputtering. For device S2, no Ti layer was deposited. The final devices were obtained after a lift-off process. Memory device structure and thicknesses of all layers were observed by transmission electron microscopy (TEM) with an energy of 200 keV. The TaO_x material was also confirmed by quadrupole secondary ion mass spectroscopy (SIMS; ATOMIKA SIMS 4500, MA-Tek, Hsinchu, Taiwan) which had a high depth resolution. Primary beam was O²⁺ with an energy of 0.5 keV and analysis area of 37.5×37.5 μm^2 . A bias was applied to the TE, and the BE was electrically grounded. Pristine S1 and S2 devices were electroformed by applying positive voltage to the TE before consecutive resistive switching cycle measurements.

Results and discussion

Figure 1a shows a typical cross-sectional TEM image of the W/TiO_x/TaO_x/W structure. The device size is 150×150 nm². HRTEM images of the S1 and S2 devices are shown in Figure 1b,c. The thicknesses of the TiO_x and

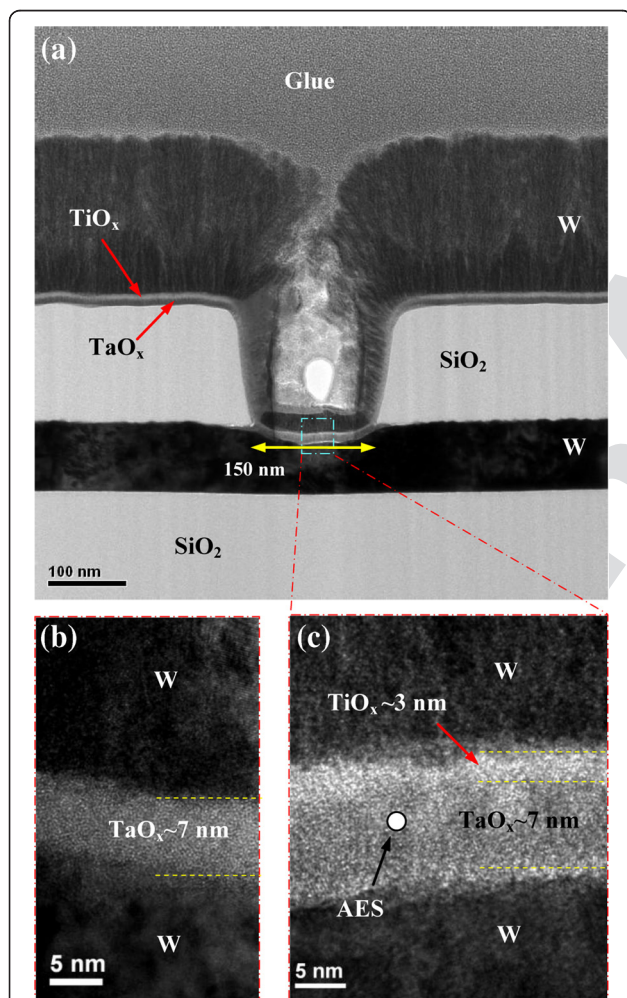


Figure 1 TEM and HRTEM images of W/TiO_x/TaO_x/W (S1) and W/TaO_x/W (S2) structures. (a) TEM image of fabricated W/TiO_x/TaO_x/W (S1) structure. HRTEM images of (b) W/TaO_x/W (S2) and (c) S1 structures. AES spectra of the TaO_x layer were measured at the point marked in (c), before and after switching of the S1 memory devices.

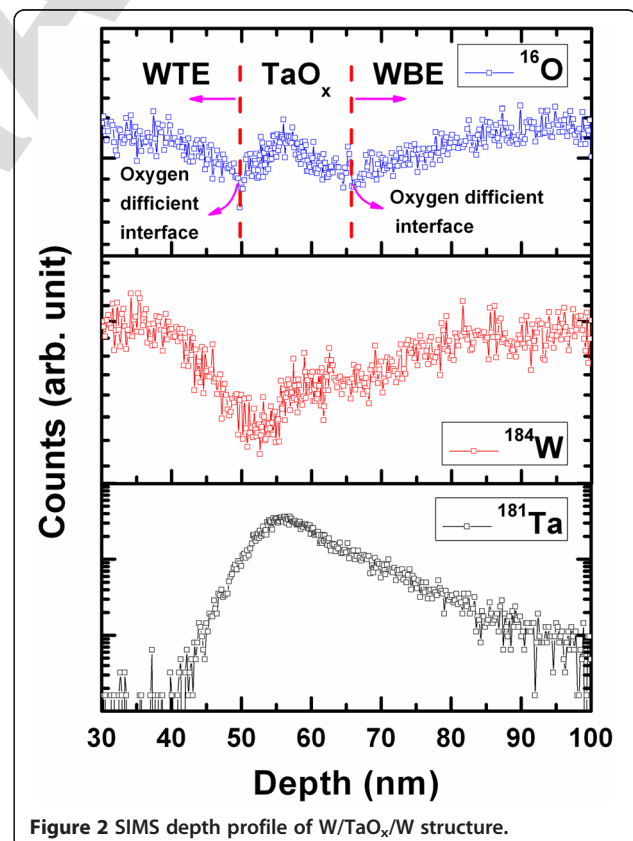


Figure 2 SIMS depth profile of W/TaO_x/W structure.

TaO_x layers are approximately 3 and 7 nm, respectively, and both films show an amorphous characteristic. Figure 2 shows typical SIMS depth profiles of ¹⁶O, ¹⁸⁴W, and ¹⁸¹Ta materials. The thickness of the TaO_x layer is about 15 nm; however, this is higher than the deposited film thickness of 7 nm. This is due to the trail effect and surface roughness of W BE, as we can see from the depth of 57 to 65 nm (or approximately 7 nm) of the ¹⁸⁴W depth profile. It is interesting to note that the TaO_x/W interface is found to be an oxygen-deficient layer, which makes it a more conducting interface. On the other hand, the conducting filament will be formed after breaking the

Ta-O bonds in the bulk Ta₂O₅ layer rather than the W/TaO_x interface. This is because the Ta₂O₅ layer is more insulating than the W/TaO_x interface, so the electric field will drop across the Ta₂O₅ film rather than the W/TaO_x interface which probably results into multi-filaments or an uncontrolled nanofilament diameter. As Ti removes oxygen from the Ta₂O₅ film in the W/TiO_x/TaO_x/W structure, the film becomes more oxygen-deficient TaO_x, which is vital to achieve an improved resistive switching. Considering Gibbs free energies of TiO₂, Ta₂O₅, and WO₃ films, which are -887.6, -760.5, and -506.5 kJ/mol, respectively, at 300 K [35], Ti will consume the highest

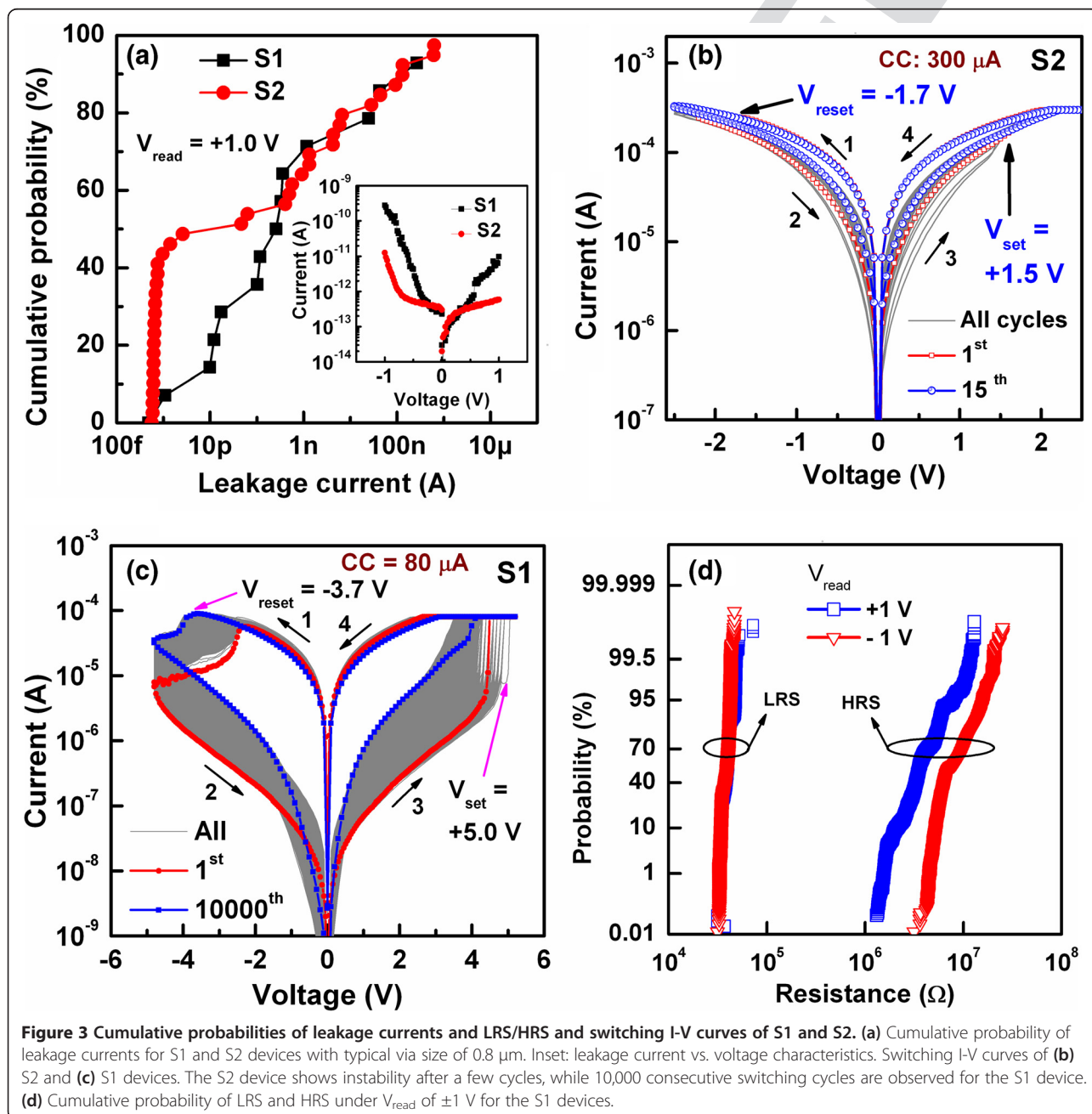
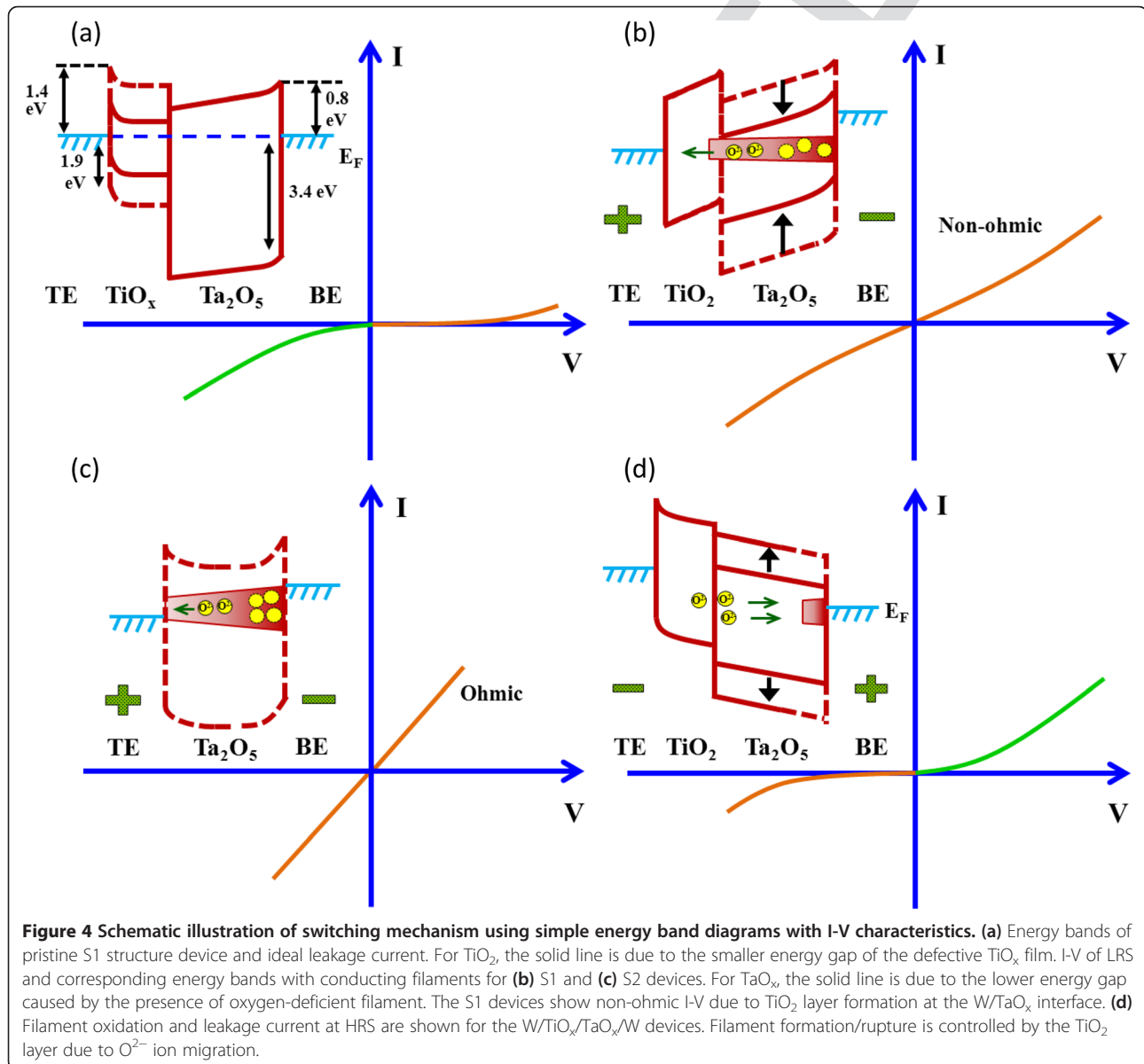


Figure 3 Cumulative probabilities of leakage currents and LRS/HRS and switching I-V curves of S1 and S2. (a) Cumulative probability of leakage currents for S1 and S2 devices with typical via size of 0.8 μm. Inset: leakage current vs. voltage characteristics. Switching I-V curves of (b) S2 and (c) S1 devices. The S2 device shows instability after a few cycles, while 10,000 consecutive switching cycles are observed for the S1 device. (d) Cumulative probability of LRS and HRS under V_{read} of ±1 V for the S1 devices.

oxygen content owing to its stronger reactivity than those of the other materials, thereby forming a Ta-rich (or defective TaO_x) film. This also prevents oxidation of the W TE at the TaO_x/W interface of device S1 owing to the migration of oxygen from the underlying films towards the Ti film, which contributes to the improved resistive switching memory performance as will be described.

The leakage current values of most of the S1 pristine devices at a read voltage (V_{read}) of 1 V are higher than that of the S2 devices because of the presence of more oxygen vacancies in the TaO_x layer owing to the oxygen-getter nature of the TiO_x layer (Figure 3a). Typical current-voltage ($I-V$) curves (inset of Figure 3a) of both devices were asymmetrical with higher current at a negative voltage (≈ 281 pA for S1 and ≈ 12.6 pA for S2 at

$V_{read} = -1$ V) compared with that measured at a positive voltage (≈ 9.8 pA for S1 and ≈ 0.6 pA for S2 at $V_{read} = 1$ V). This suggests that the W TE/ TaO_x interface has more oxygen vacancies than the TaO_x/W BE interface, owing to oxygen migration towards W TE during deposition. The ideal leakage current is plotted in Figure 4a and is explained as follows. It is reported that the work function (Φ_m) of W and bandgap (E_g) of amorphous Ta_2O_5 and TiO_2 are 4.55 [36], 4.2 [37], and 3.3 eV [38], respectively. The conduction band offsets of Ta_2O_5 and TiO_2 with Si are 0.3 [39] and 0.9 eV [40], respectively. Taking the electron affinity of Si as 4.05 eV, the electron affinities of Ta_2O_5 and TiO_2 are calculated to be 3.75 and 3.15 eV, respectively. The corresponding energy diagram is shown in Figure 4a as solid lines. Considering that the E_g of TiO_2



for the pristine S1 device will be much lower because of oxygen vacancy creation during the deposition of W TE, the band diagram is shown in dotted lines (Figure 4a). In this case, electron injection dominates rather than hole injection because of a lower barrier height for electrons than for holes (0.8 to 1.4 vs. 3.4 eV). Both S1 and S2 devices show bipolar resistive switching behaviors. The S2 device shows few switching cycles with a higher leakage current of $\approx 10 \mu\text{A}$ at $V_{\text{read}} = 1 \text{ V}$ and a higher CC of $300 \mu\text{A}$ (Figure 3b). In this case, negatively charged oxygen ions (O^{2-}) migrate from the switching material towards W TE, and this has a lesser possibility to form an oxygen-rich layer at the W TE/ TaO_x interface, leading to the formation of multi-conduction filaments. In the same way, no resistive switching is observed under negative forming voltage for either the S1 or S2 devices because oxygen ions migrate towards the W BE and permanent breakdown is observed (not shown here). However, the insertion of a thin ($\approx 3 \text{ nm}$) Ti layer in between the W and TaO_x layers in the S1 device makes a vast difference because Ti can be used as an oxygen reservoir. Moreover, the S1 device exhibits $>10,000$ consecutive repeatable dc switching cycles with a better resistance ratio of 10^2 under a low CC of $80 \mu\text{A}$ (Figure 3c). However, a thicker Ti layer (5 nm) results in unstable switching cycles because it gets more oxygen and behaves as an insulating layer. This indicates that the thinner (3 nm) Ti layer will control the current overflow as well as will control the filament diameter. The yield of the S1 device is very high ($>95\%$), while that of the S2 device is very low (approximately 10%). In addition, the S2 device cannot be switched below a CC of $300 \mu\text{A}$ and shows an ohmic behavior, while the S1 device shows switching even at a low CC of $10 \mu\text{A}$ (discussed later) with non-ohmic current conduction. The average values and standard deviation/average are found to be 39.7 and 0.11, 38.4 k Ω and 0.08 for low-resistance state (LRS) and 1.9 and 2.11, 8.6 M Ω and 0.43, for high-resistance state (HRS) at V_{read} of 1 V and -1 V , respectively (Figure 3d). This suggests that the LRS has a tighter distribution than the HRS because of the formation of the TiO_2 layer, which will have a higher E_g than the pristine one. Similarly, the leakage current at V_{read} of -1 V is lower than that at $+1 \text{ V}$ because of the lower electron injection barrier at the TE/ TiO_2 interface than that at the BE/ TaO_x interface after switching. Under 'SET', O^{2-} rather than oxygen vacancies will migrate from TaO_x towards the TE, resulting in a TiO_2 layer which controls the conducting vacancy filament diameter in the TaO_x layer by controlling current overflow and producing a tighter distribution of the LRS (Figure 4b). Owing to this series resistance, the S1 devices exhibit non-ohmic-simulated ideal current, as shown in Figure 4b, whereas an ohmic current is observed for the S2 devices under SET (Figure 4c). It is true that the conducting filament is formed through the TaO_x film

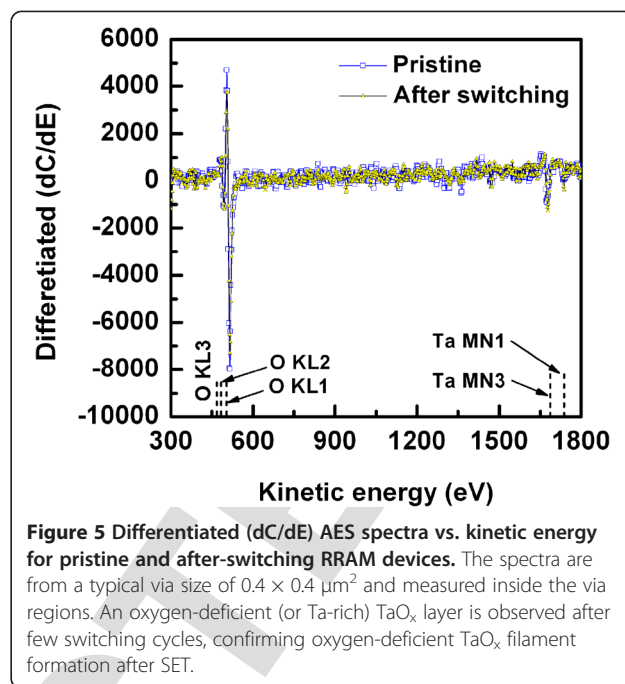


Figure 5 Differentiated (dC/dE) AES spectra vs. kinetic energy for pristine and after-switching RRAM devices. The spectra are from a typical via size of $0.4 \times 0.4 \mu\text{m}^2$ and measured inside the via regions. An oxygen-deficient (or Ta-rich) TaO_x layer is observed after few switching cycles, confirming oxygen-deficient TaO_x filament formation after SET.

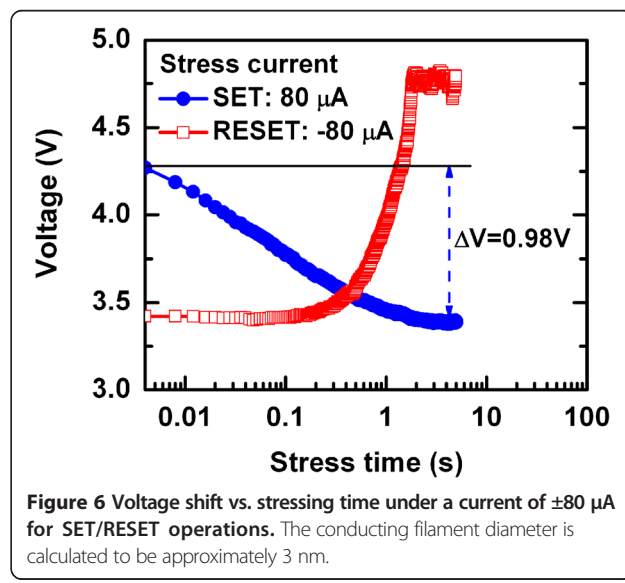


Figure 6 Voltage shift vs. stressing time under a current of $\pm 80 \mu\text{A}$ for SET/RESET operations. The conducting filament diameter is calculated to be approximately 3 nm.

rather than oxygen vacancy migration as well as the lower energy gap of the TaO_x layer, as shown by the dotted line in Figure 4b. When negative voltage is applied to the TE, oxygen ions are pushed from the TiO₂ layer towards the conducting filament where they recombine with oxygen vacancies or oxidize the conducting filament. The device will be in HRS (Figure 4d). Control of oxygen-deficient filament formation and rupture is facilitated by insertion of the thin Ti layer at the TE/TaO_x interface, which results in repeatable and reproducible resistive switching characteristics.

The conducting filament diameter is estimated using a new method under a constant current stress of 80 μA (Figure 6). The voltage decreases (or increases) under positive (or negative) current stress after a SET (or RESET) operation. Under SET, the oxygen ions formed by the breakage of Ta-O bonds migrate towards the TiO_x layer and create an oxygen-deficient (or conducting path) in the TaO_x layer. Assuming a cylindrical nanofilament, the diameter (*D*) can be estimated as [41]:

$$D = \sqrt{\frac{4 \cdot q \cdot t_{\text{Ta}_2\text{O}_5}}{\pi \cdot \epsilon_{\text{Ta}_2\text{O}_5} \cdot \Delta V}} \quad (1)$$

where Δ*V* (changes in the voltage shift) is found to be 0.98 V (Figure 6), *q* is the electronic charge (1.602 × 10⁻¹⁹ C), and ε_{Ta₂O₅} is the dielectric permittivity of amorphous Ta₂O₅ film (ε_{Ta₂O₅} ≈ 20 to 25). Considering all values in Equation 1, the diameter of the nanofilament is approximately 2.9 to 2.6 nm. This suggests that the present resistive switching memory device can be scaled down to <3 nm. Previously reported diameters of 5 to 10 nm for Pt/TiO₂/Pt [12], ≈15 nm for Ti/Fe:SrTiO₃/Nb:SrTiO₃ [37], and ≈1,000 nm for Pt/CuO/Pt [42] are slightly closer and higher than our calculated values, likely owing to the use of different structures as well as materials. Further study may be needed to clearly understand these results. Figure 7a shows the resistive switching characteristics with different CCs from 10 to 100 μA. The low-resistance state decreases with increasing CCs from 10 to 100 μA (Figure 7a,b), which will be useful for multi-level data storage applications. As the filament diameter increases with higher CCs, the low-resistance state decreases, and the value of RESET voltage increases. The RESET current can be scaled down to 23 μA at a low CC of 10 μA, which will be useful to a low-power operation RRAM in the near future. Our novel device also has a long read pulse endurance of >10⁵ cycles and excellent data retention of >10⁴ s with a good resistance ratio of >10² at 85°C at a low CC of 80 μA, as shown in Figure 8. A data retention of >10³ s is also observed for a low CC of 10 μA (not shown here). Considering the obtained nanofilament diameter of approximately 3 nm, a high-density (≈100 Tbit/in.²) nanoscale nonvolatile memory can be achievable in future.

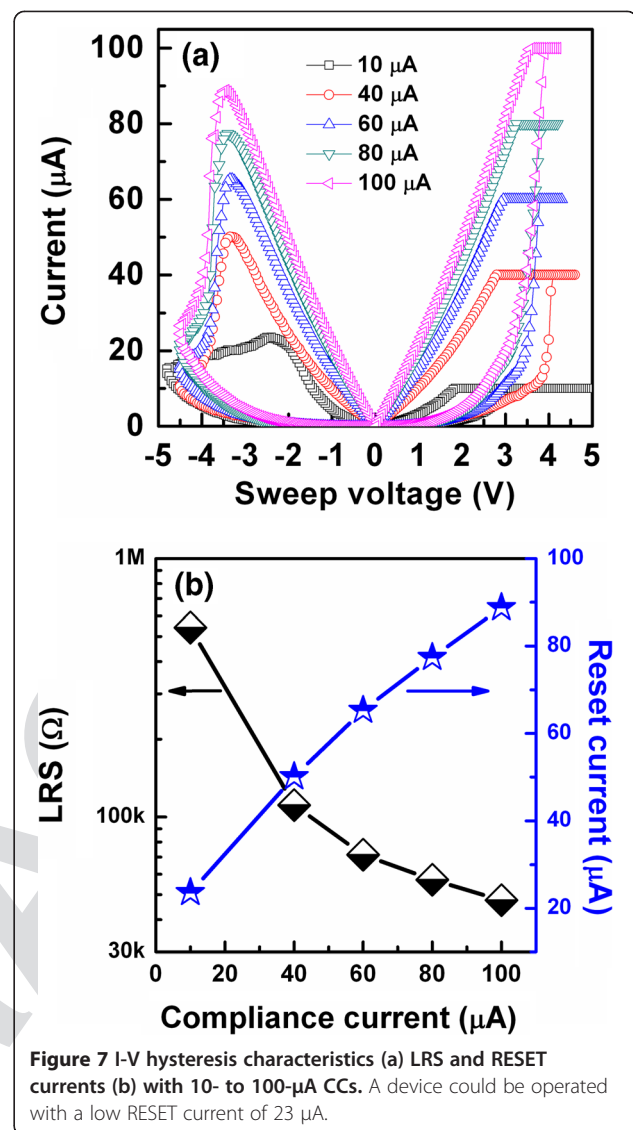


Figure 7 I-V hysteresis characteristics (a) LRS and RESET currents (b) with 10- to 100-μA CCs. A device could be operated with a low RESET current of 23 μA.

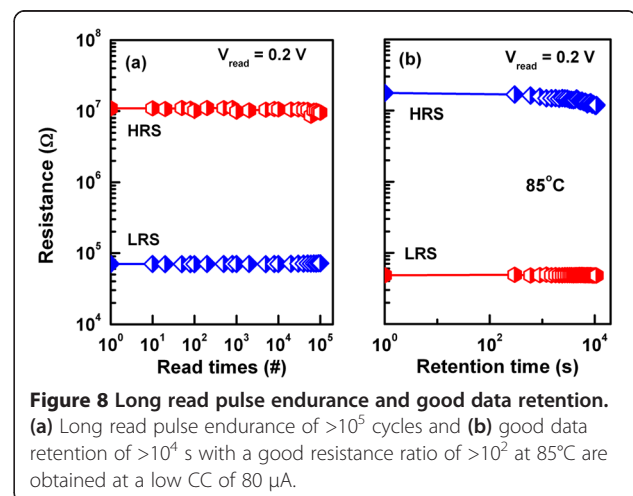


Figure 8 Long read pulse endurance and good data retention. (a) Long read pulse endurance of >10⁵ cycles and (b) good data retention of >10⁴ s with a good resistance ratio of >10² at 85°C are obtained at a low CC of 80 μA.

Conclusions

Improvement in resistive switching performance, particularly 10,000 consecutive switching cycles with tight distribution in LRS/HRS of $>10^2$, long read pulse endurance of $>10^5$, and good data retention of 10^4 s at 85°C , has been achieved under a low CC of $80\ \mu\text{A}$ by exploiting the oxygen-getter nature of a Ti nanolayer in a $\text{W}/\text{TiO}_x/\text{TaO}_x/\text{W}$ structure. A small device of $150 \times 150\ \text{nm}^2$ and a defective TaO_x film are confirmed by TEM. O^{2-} ion migration rather than oxygen vacancy migration because of lower barrier height for electrons leads to a switching mechanism based on filament formation/rupture. The presence of controllable oxygen-deficient TaO_x nanofilament after switching has been investigated by AES. Furthermore, the device could be operated with a small RESET current of $23\ \mu\text{A}$. A small nanofilament diameter of $3\ \text{nm}$ under a low CC of $80\ \mu\text{A}$ has been calculated using a new method, which has a high memory density of $\approx 100\ \text{Tbit}/\text{in.}^2$, expected to be very useful for future sub-10-nm applications.

Competing interests

The authors declare that they have no competing interests.

Authors' contributions

AP carried out this research work under the instruction of SM. Fabrication process was also instructed by HCC and CSL. AES spectra were taken by TCT under the instruction of SM. All authors read and approved the final manuscript.

Acknowledgments

This work was supported by the National Science Council (NSC), Taiwan, under contract numbers NSC-98-2221-E-182-052-MY3 and NSC-101-2221-E-182-061. The authors are grateful to Electronic and Optoelectronic Research Laboratories, Industrial Technology Research Institute, Hsinchu, Taiwan for their support on W bottom electrode pattern.

Author details

¹Department of Electronic Engineering, Chang Gung University, Tao-Yuan 333, Taiwan. ²Material and Chemical Research Laboratories, Industrial Technology Research Institute, Hsinchu 310, Taiwan.

Received: 3 May 2013 Accepted: 7 June 2013

Published: 17 June 2013

References

1. Waser R, Dittmann R, Staikov G, Szot K: Redox-based resistive switching memories - nanoionic mechanisms, prospects, and challenges. *Adv Mater* 2009, **21**:2632.
2. Sawa A: Resistive switching in transition metal oxides. *Mater Today* 2008, **11**:28.
3. Liu Q, Sun J, Lv H, Long S, Yin K, Wan N, Li Y, Sun L, Liu M: Real-time observation on dynamic growth/dissolution of conductive filaments in oxide-electrolyte-based ReRAM. *Adv Mater* 1844, 2012:24.
4. Sato Y, Kinoshita K, Aoki M, Sugiyama Y: Reduction in the reset current in a resistive random access memory consisting of NiO_x brought about by reducing a parasitic capacitance. *Appl Phys Lett* 2007, **90**:033503.
5. Lee MJ, Lee CB, Lee D, Lee SR, Chang M, Hur JH, Kim YB, Kim CJ, Seo DH, Seo S, Chung UI, Yoo IK, Kim K: A fast, high-endurance and scalable non-volatile memory device made from asymmetric $\text{Ta}_2\text{O}_{(5-x)}/\text{TaO}_{(2-x)}$ bilayer structures. *Nat Mater* 2011, **10**:625.
6. Yoon J, Choi H, Lee D, Park JB, Lee J, Seong DJ, Ju Y, Chang M, Jung S, Hwang H: Excellent switching uniformity of Cu-doped $\text{MoO}_3/\text{GdO}_x$ bilayer for nonvolatile memory applications. *IEEE Electron Device Lett* 2009, **30**:457.
7. Prakash A, Maikap S, Lai CS, Lee HY, Chen WS, Chen F, Kao MJ, Tsai MJ: Improvement uniformity of resistive switching parameters by selecting the electroformation polarity in $\text{IrO}_x/\text{TaO}_x/\text{WO}_x/\text{W}$ structure. *Jpn J Appl Phys* 2012, **51**:04DD06.
8. Banerjee W, Maikap S, Lai CS, Chen YY, Tien TC, Lee HY, Chen WS, Chen FT, Kao MJ, Tsai MJ, Yang JR: Formation polarity dependent improved resistive switching memory characteristics using nanoscale (1.3 nm) core-shell IrO_x nano-dots. *Nanoscale Res Lett* 2012, **7**:194.
9. Yoon JH, Kim KM, Lee MH, Kim SK, Kim GH, Song SJ, Seok JY, Hwang CS: Role of Ru nano-dots embedded in TiO_2 thin films for improving the resistive switching behavior. *Appl Phys Lett* 2010, **97**:232904.
10. Lee HY, Chen PS, Liu WH, Wang SM, Gu PY, Hsu YY, Tsai CH, Chen WS, Chen F, Tsai MJ, Lien C: Robust high-resistance state and improved endurance of HfO_x resistive memory by suppression of current overshoot. *IEEE Electron Device Lett* 2011, **32**:1585.
11. Choi BJ, Jeong DS, Kim SK, Rohde C, Choi S, Oh JH, Kim HJ, Hwang CS, Szot K, Waser R, Reichenberg B, Tiedke S: Resistive switching mechanism of TiO_2 thin films grown by atomic-layer deposition. *J Appl Phys* 2005, **98**:033715.
12. Kwon DH, Kim KM, Jang JH, Jeon JM, Lee MH, Kim GH, Li XS, Park GS, Lee B, Han S, Kim M, Hwang CS: Atomic structure of conducting nanofilaments in TiO_2 resistive switching memory. *Nat Nanotechnol* 2010, **5**:148.
13. Lee SR, Char K, Kim DC, Jung R, Seo S, Li XS, Park GS, Yoo IK: Resistive memory switching in epitaxially grown NiO . *Appl Phys Lett* 2007, **91**:202115.
14. Yu S, Guan X, Wong HSP: Conduction mechanism of $\text{TiN}/\text{HfO}_2/\text{Pt}$ resistive switching memory: a trap-assisted-tunneling model. *Appl Phys Lett* 2011, **99**:063507.
15. Chen YY, Goux L, Clima S, Govoreanu B, Degraeve R, Kar GS, Fantini A, Groeseneken G, Wouters DJ, Jurczak M: Endurance/retention trade-off on $\text{HfO}_2/\text{metal cap}$ 1T1R bipolar RRAM. *IEEE Trans Electron Devices* 2013, **60**:1114.
16. Lin CY, Wu CY, Wu CY, Lee TC, Yang FL, Hu C, Tseng TY: Effect of top electrode material on resistive switching properties of ZrO_2 film memory devices. *IEEE Electron Device Lett* 2007, **28**:366.
17. Guan W, Long S, Jia R, Liu M: Nonvolatile resistive switching memory utilizing gold nanocrystals embedded in zirconium oxide. *Appl Phys Lett* 2007, **91**:062111.
18. Liu Q, Guan W, Long S, Liu M, Zhang S, Wang Q, Chen J: Resistance switching of Au-implanted- ZrO_2 film for nonvolatile memory application. *J Appl Phys* 2008, **104**:114514.
19. Wang SY, Lee DY, Tseng TY, Lin CY: Effects of Ti top electrode thickness on the resistive switching behaviors of rf-sputtered ZrO_2 memory films. *Appl Phys Lett* 2009, **95**:112904.
20. Wang SY, Lee DY, Huang TY, Wu JW, Tseng TY: Controllable oxygen vacancies to enhance resistive switching performance in a ZrO_2 -based RRAM with embedded Mo layer. *Nanotechnology* 2010, **21**:495201.
21. Li Y, Long S, Lv H, Liu Q, Wang Y, Zhang S, Lian W, Wang M, Zhang K, Xie H, Liu S, Liu M: Improvement of resistive switching characteristics in ZrO_2 film by embedding a thin TiO_x layer. *Nanotechnology* 2011, **22**:254028.
22. Lin CC, Chang YP, Lin HB, Lin CH: Effect of non-lattice oxygen on ZrO_2 -based resistive switching memory. *Nanoscale Res Lett* 2012, **7**:187.
23. Zhang T, Zhang X, Ding L, Zhang W: Study on resistance switching properties of $\text{Na}_{0.5}\text{Bi}_{0.5}\text{TiO}_3$ thin films using impedance spectroscopy. *Nanoscale Res Lett* 2009, **4**:1309.
24. Sun X, Li G, Chen L, Shi Z, Zhang W: Bipolar resistance switching characteristics with opposite polarity of $\text{Au}/\text{SrTiO}_3/\text{Ti}$ memory cells. *Nanoscale Res Lett* 2011, **6**:599.
25. Chiu FC, Li PW, Chang WY: Reliability characteristics and conduction mechanisms in resistive switching memory devices using ZnO thin films. *Nanoscale Res Lett* 2012, **7**:178.
26. Peng CN, Wang CW, Chan TC, Chang WY, Wang YC, Tsai HW, Wu WW, Chen LJ, Chueh YL: Resistive switching of $\text{Au}/\text{ZnO}/\text{Au}$ resistive memory: an *in situ* observation of conductive bridge formation. *Nanoscale Res Lett* 2012, **7**:559.
27. Rahaman SZ, Maikap S, Chen WS, Lee HY, Chen FT, Kao MJ, Tsai MJ: Repeatable unipolar/bipolar resistive memory characteristics and switching mechanism using a Cu nanofilament in a GeO_x film. *Appl Phys Lett* 2012, **101**:073106.
28. Syu YE, Chang TC, Tsai TM, Chang GW, Chang KC, Lou JH, Tai YH, Tsai MJ, Wang YL, Sze SM: Asymmetric carrier conduction mechanism by tip

- electric field in WSiO_x resistance switching device. *IEEE Electron Device Lett* 2012, **33**:342.
29. Rahaman SZ, Maikap S, Tien TC, Lee HY, Chen WS, Chen F, Kao MJ, Tsai MJ: **Excellent resistive memory characteristics and switching mechanism using a Ti nanolayer at the Cu/TaO_x interface.** *Nanoscale Res Lett* 2012, **7**:345.
 30. Prakash A, Maikap S, Lai CS, Tien TC, Chen WS, Lee HY, Chen FT, Kao MJ, Tsai MJ: **Bipolar resistive switching memory using bilayer TaO_x/WO_x films.** *Solid State Electron* 2012, **77**:35.
 31. Chen C, Song C, Yang J, Zeng F, Pan F: **Oxygen migration induced resistive switching effect and its thermal stability in W/TaO_x/Pt structure.** *Appl Phys Lett* 2012, **100**:253509.
 32. Terai M, Sakotsubo Y, Kotsuji S, Hada H: **Resistance controllability of Ta₂O₅/TiO₂ stack ReRAM for low-voltage and multilevel operation.** *IEEE Electron Device Lett* 2010, **31**:204.
 33. Ninomiya T, Wei Z, Muraoka S, Yasuhara R, Katayama K, Takagi T: **Conductive filament scaling of TaO_x bipolar ReRAM for improving data retention under low operation current.** *IEEE Trans Electron Devices* 2013, **60**:1384.
 34. Wei Z, Kanzawa Y, Arita K, Katoh Y, Kawai K, Muraoka S, Mitani S, Fujii S, Katayama K, Iijima M, Mikawa T, Ninomiya T, Miyanaga R, Kawashima Y, Tsuji K, Himeno A, Okada T, Azuma R, Shimakawa K, Sugaya H, Takagi T, Yasuhara R, Horiba K, Kumigashira H, Oshima M: **Highly reliable TaO_x ReRAM and direct evidence of redox reaction mechanism.** *Tech Dig - Int Electron Devices Meet* 2008, **293**:293.
 35. **The interactive Ellingham diagram.** [http://www.doitpoms.ac.uk/tlplib/ellingham_diagrams/interactive.php]
 36. Michaelson HB: **The work function of the elements and its periodicity.** *J Appl Phys* 1977, **48**:4729.
 37. Stille S, Lenser C, Dittmann R, Koehl A, Krug I, Muenstermann R, Perlich J, Schneider CM, Klemradt U, Waser R: **Detection of filament formation in forming-free resistive switching SrTiO₃ devices with Ti top electrodes.** *Appl Phys Lett* 2012, **100**:223503.
 38. Aarik J, Aidla A, Kiisler AA, Uustare T, Sammelselg V: **Effect of crystal-structure on optical-properties of TiO₂ films grown by atomic layer deposition.** *Thin Solid Films* 1997, **305**:270.
 39. Gu D, Li J, Dey SK, Waard HD, Marcus S: **Nanochemistry, nanostructure, and electrical properties of Ta₂O₅ film deposited by atomic layer deposition and plasma-enhanced atomic layer deposition.** *J Vac Sci Technol B* 2006, **24**:2230.
 40. Maikap S, Wang TY, Tzeng PJ, Lin CH, Tien TC, Lee LS, Yang JR, Tsai MJ: **Band offsets and charge storage characteristics of atomic layer deposited high-k HfO₂/TiO₂ multilayers.** *Appl Phys Lett* 2007, **90**:262901.
 41. Prakash A, Maikap S, Rahaman SZ, Majumdar S, Manna S, Ray SK: **Resistive switching memory characteristics of Ge/GeO_x nanowires and evidence of oxygen ion migration.** *Nanoscale Res Lett* 2013, **8**:220.
 42. Yasuhara R, Fujiwara K, Horiba K, Kumigashira H, Kotsugi M, Oshima M, Takagi H: **Inhomogeneous chemical states in resistance-switching devices with a planar-type Pt/CuO/Pt structure.** *Appl Phys Lett* 2009, **95**:012110.

doi:10.1186/1556-276X-8-288

Cite this article as: Prakash et al.: Enhanced resistive switching memory characteristics and mechanism using a Ti nanolayer at the W/TaO_x interface. *Nanoscale Research Letters* 2013 **8**:288.

Submit your manuscript to a SpringerOpen[®] journal and benefit from:

- Convenient online submission
- Rigorous peer review
- Immediate publication on acceptance
- Open access: articles freely available online
- High visibility within the field
- Retaining the copyright to your article

Submit your next manuscript at ► springeropen.com